Hindawi
Geofluids
Volume 2022, Article ID 1279642, 13 pages
https://doi.org/10.1155/2022/1279642

Research Article

Floor Disturbance and Failure Characteristics of Super-Large Mining Height Working Face

Cunjin Lu,[1] Jinpeng Xu,[1] Hui Zhao,[1] Heng Zhang,[1] Yian Zhang,[2] and Mingyue Chen[1]

[1]*School of Resources and Geosciences, China University of Mining and Technology, Xuzhou, Jiangsu 221116, China*
[2]*Inner Mongolia Erdos Guoyuan Mining Development Co., LTD., Longwanggou Coal Mine, Ordos, Inner Mongolia 017000, China*

Correspondence should be addressed to Jinpeng Xu; xujinpengcumt@163.com

Received 25 November 2021; Revised 25 February 2022; Accepted 11 March 2022; Published 9 April 2022

Academic Editor: Wensong Wang

The failure depth of the working face floor caused by mining is a key parameter to predict water inrush from the working face floor. Extensive research has been conducted on the floor failure zone of the working face. However, in recent years, there have been few studies on the floor failure law of the working face with a super-large mining height (over 20 m) in the western mining area of China. In this paper, the working face with a super-large mining height of 24 m in Longwanggou Coal Mine was studied. Electrical monitoring and numerical simulation of the working face floor were carried out. The measured floor failure depth of the working face is 15 m while the average numerical simulation result is 11 m. When compared with the calculation results of the statistical analysis formulas, the floor failure depth of the working face with a super large mining height obtained from field measurement and numerical simulation is smaller. The reason for the smaller failure zone of the floor of the super large mining height working face is that the falling roof inhibits the pressure relief of the floor, the large mining height reduces the advance pressure, and the shear stress of the floor decreases. The research methods and findings are of great significance to the prediction of floor failure and water inrush in working face with a super-large mining height, the prevention and control of water disasters in coal seam roof and the monitoring of mine pressure.

1. Introduction

More than 90% of China's coal production comes from Carboniferous-Permian and Jurassic coalfields in North China. The basement of the Carboniferous-Permian coalfield in North China is the Ordovician karst-rich aquifer. All the mining areas in the east of the Taihang Mountains are mined under the Ordovician karst confined water surface. With the extension of mining in the mining area in the west of the Taihang Mountains, most mines have been transferred to the Ordovician karst confined water surface. In the vast North China coalfield, many mines have been transferred from the Permian and Jurassic (such as Datong) coal seam mining to the Carboniferous coal seam mining. The floor of the Carboniferous coal seam is close to the Ordovician roof, and the water pressure of the Ordovician aquifer is high. In the process of mining, water inrush is often caused by the destruction of the floor of the working face. As one of the important water disasters in China's coal mines, the water damage of the floor of the working face often causes flooding areas or even flooding accidents, which poses a great threat to the safety of miners' lives and properties, and brings great damage to the natural environment. Therefore, it is of great significance to study of the development characteristics of the floor failure zone of the working face for controlling the water inrush from the coal mine floor.

Since the theory of "lower three zones" was proposed by Li and Mi [1, 2], understanding the floor failure zone of working face has become the core issue of floor water inrush research. The field measurement methods for studying floor failure have evolved from initial water injection experiments [3], floor stress and strain observations [4], to various physical observation methods [5] such as electrical observations of working face floor [6], seismic methods [7], and borehole resistivity measurements [8]. The distributed optical fiber sensing technology (BOTDR) and three-dimensional resistivity method were used for field measurements [9]. A

microseismic monitoring system was constructed to realize three-dimensional visualization and real-time perception of the initiation and expansion of floor microfailure [10]. A fluid-solid coupling material model was established to study the evolution and failure characteristics of floor cracks in confined water mining [11]. The evolution characteristics of strain field and geoelectric field under mining conditions were compared and analyzed to reveal the development mechanism of rock deformation and failure [12]. At the same time, many researchers have used different software to carry out numerical simulations under different conditions [10, 13]. The critical conditions for bending and contracting during mining were analyzed by FLAC-3D numerical simulation [14]. Indoor material simulation under different conditions was also a commonly used research method [15]. A failure test system of coal mining floor in confined water was developed for simulation [16].

Through the above literature research, it is found that the main factor affecting the floor failure of the working face is the width of the working face. The empirical formulas for the floor failure zone of the working face proposed by many researchers are related to the width of the working face [17, 18]. It was also suggested in some literature that the floor failure zone of the working face is related to the burial depth of the coal seam, the dip angle of the coal seam, the mining method, the mining height, and other factors [19–22]. In addition, the microscopic characteristics of rock mass also determine its damage characteristics. Hilbert-Huang transform (HHT) method was used to obtain the detailed structural characteristics of coal and rock mass related to damage at different loading stages, which can provide a basis for coal rock dynamic disaster monitoring [23].

In recent years, with the depletion of coal resources in the eastern mining area and the intensification of the contradiction between resource development and environmental protection in the central region, the focus of coal resource development in China has been rapidly transferred to the western region. The main characteristics of coal resources in the western mining area are that thick coal seams are widely distributed and that there are many super-thick coal seams. For example, Zhundong Coalfield, the largest integrated coalfield in China and even in the world, has super-thick coal seams with a single-layer thickness of more than 80 m, and the thickness of single-layer coal seam in Shaerhu Coalfield is even more than 200 m. Based on the above background investigation, coal caving mining of super-thick coal seams with a large mining height over 20 m has occurred in some western mining areas. The mining pressure generated by coal caving mining of super-thick coal seams will be much greater than that of normal mining height coal seams, which directly leads to more complex development characteristics of the floor failure zone, greater failure depth, and higher probability of water inrush accidents in floor aquifers. However, there are few studies on the development characteristics of the floor failure zone in the working face with a large mining height over 20 m, and the law of the floor failure zone is not very clear. For example, the relationship between the mining height and the floor failure zone of the working face was explored, but within the mining height range of 1.0 m to 3.5 m [22]. The characteristics of the floor failure zone of the extra-thick coal seam with a thickness of 6.20~10.40 m were examined [24]. The caving characteristics of rock and the height of the water flowing fractured zone in fully mechanized caving mining of extra-thick coal seams were theoretically analyzed [25], and the roof failure characteristics and mining pressure behavior law of fully mechanized caving face with a large mining height were studied [26].

In this paper, the floor failure characteristics of the working face with a mining height of over 20 m in the west were studied. The network parallel electrical monitoring method used in this study is also applied to the study of the development law of the roof water flowing fractured zone and the variation law of the roof and floor stratum pressure during the mining of the working face, which has the same important significance for the prevention and control of roof water disasters and the monitoring of stratum pressure.

2. Research Methods and Procedures

2.1. Overview of Longwanggou Coal Mine. Longwanggou Coal Mine is located in the north-central part of Zhungeer Coalfield, 120 kilometers east of Ordos City, Inner Mongolia Autonomous Region. The Mesozoic stratigraphic region of the mine belongs to the Dongsheng stratigraphic minor region of the Ordos stratigraphic subregion. The stratigraphic sequence of this mine from bottom to top is as follows: Middle Ordovician Majiagou Formation (O_{2m}), Upper Carboniferous Taiyuan Formation (C_{2t}), Lower Permian Shanxi Formation (P_{1s}), Lower Shihezi Formation (P_{1x}), Upper Shihezi Formation (P_{2s}), Shiqianfeng Formation (P_{2sh}), Lower Triassic Liujiagou Formation (T_{1l}), Neogene Pliocene (N_2), and Quaternary System (Q). This mine is located on the monoclinic structure on the northwestern wing of the West Huangjialiang anticline. The strata strike nearly north-south and incline to the west with dip angles mostly below 5°.

The mining of this mine occurs mainly in the No. 6 coal seam. The natural thickness of this coal seam is 4.00~35.55 m with an average of 21.72 m. For the 61601 working face in this study (plan view, see Figure 1), the coal seam has a thickness of 19.8~27.6 m with an average of 24 m, a dip angle of 2°, and a buried depth of 340~383.9 m.

The floor of the working face is sandy mudstone of the Taiyuan Formation (see the left side of Figure 2), under which is the Ordovician limestone karst fissured aquifer, which is a strong aquifer rich in water locally. The floor of the working face is 44.5 m away from the Ordovician limestone roof interface, and the Ordovician limestone water head pressure is 0.24 MPa. Therefore, it is necessary to monitor the floor failure zone to prevent the occurrence of water inrush from the Ordovician limestone during the mining process on the working face.

2.2. Field Measurement of Floor Failure of Working Face

2.2.1. Principle of Network Parallel Electric Method for Identifying Depth of Floor Failure Zone. The stress

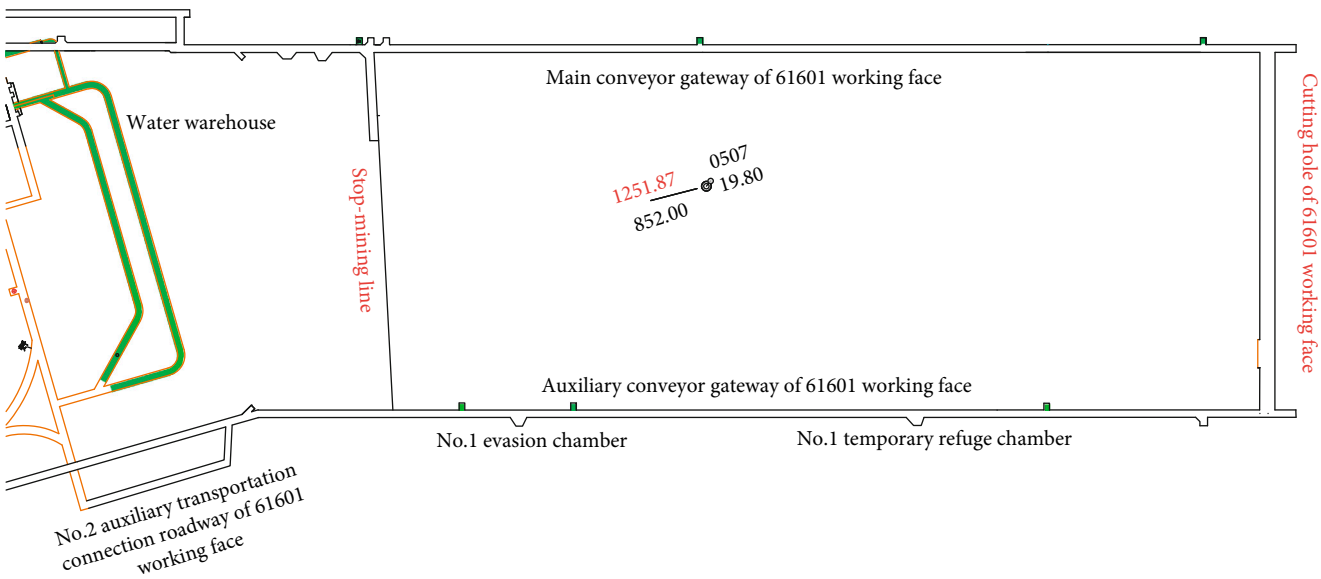

Figure 1: Plan view of the 61601 working face.

distribution of the floor rock of the working face changes under the influence of mining-induced failure, which leads to the failure of the rock mass and the formation of a plastic failure zone. The corresponding performance is a dramatic change in parameters such as natural potential. The cracks in the floor failure zone seen as the resistivity of the plastic failure zone of the floor are significantly increased due to the filling of gas. Moreover, it is difficult for the resistivity of the working face after mining to reach the state before the failure under the recompaction. In addition, in the deep plastic failure zone, the rock mass deforms but does not damage under the action of external force. After the working face is mined, the stress disappears and the deformation of the rock mass recovers. The corresponding performance is that the changes of parameters such as natural potential are relatively small, and the resistivity data can basically be restored to their original state. Based on this, the depth of the mining failure zone for floor failure can be determined [27, 28].

In view of the complexity of floor failure mechanism and the limitation of floor water inrush evaluation, in this study, the resistivity change is used as the main criterion to judge the floor failure zone of the working face, and the natural potential is used as an auxiliary judgment parameter. However, in this study, measurements were made only done in some areas of the 61601 working face, and the measurement area is not large enough. Moreover, only one measurement method was used, and the measurement results cannot be compared with those by other measurement methods. In addition, there are few data of mines with large mining heights in China at present, and it is impossible to carry out large-scale statistics to improve the empirical formula, which is the limitation of this study.

2.2.2. Observation Method and Arrangement. According to the *Test Method for Dynamic Apparent resistivity of Overburden failure in Coal Mining of the Energy Industry standard of the People's Republic of China, NB/T 51035-2015*, the floor failure zone of the working face was monitored. The network parallel electrical method was used to observe the resistivity and natural potential to determine the depth and location of the floor failure. The instrument used for monitoring is intrinsically safe explosion-proof YBD-11 network parallel electrical instrument. A three-dimensional observation system that combines boreholes and tunnels was adopted for the measuring wire layout, as shown in Figure 3.

#1 and #2 measuring wires were for tunnels. Each of them had 16 electrodes with a total of 32 electrodes. The total control length of the two measuring wires was 169 m. #3 measuring wire was for boreholes, and it had 16 electrodes with an electrode spacing of 3.5 m. The actual control length of this measuring wire was 52.5 m, and the effective control depth was 34.43 m under the floor. The three measuring wires above form a three-dimensional network observation system.

2.2.3. Observation Procedure and Results. The equipment installation was completed after debugging of the network and power supply, as shown in Figure 4. The data collection was started on April 15, 2019. At this time, the shortest distance between the mining location and the measuring wires is 85.7 m. When the mining of the working face was completed on October 23, 2019, the data collection was ended. During the monitoring period, the data were collected regularly four times a day.

The collected data was processed on the processing platform of the special "WBDPro resistivity data analysis system," as shown in Figure 5. The apparent resistivity and correlation diagram as well as an inversion model closer to the true resistivity were obtained, and the natural potential was also obtained.

AM and ABM in the data processing flow chart are two data acquisition methods, and the two data can be extracted

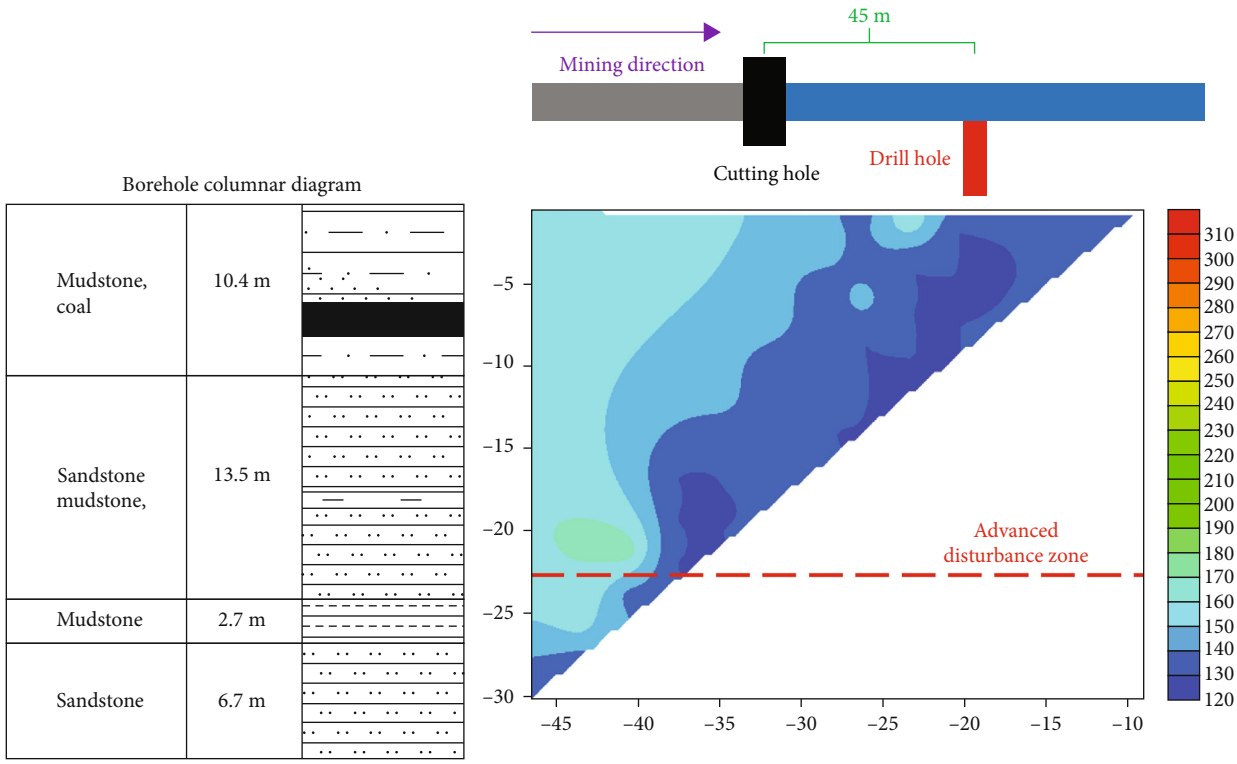

(a) On July 2

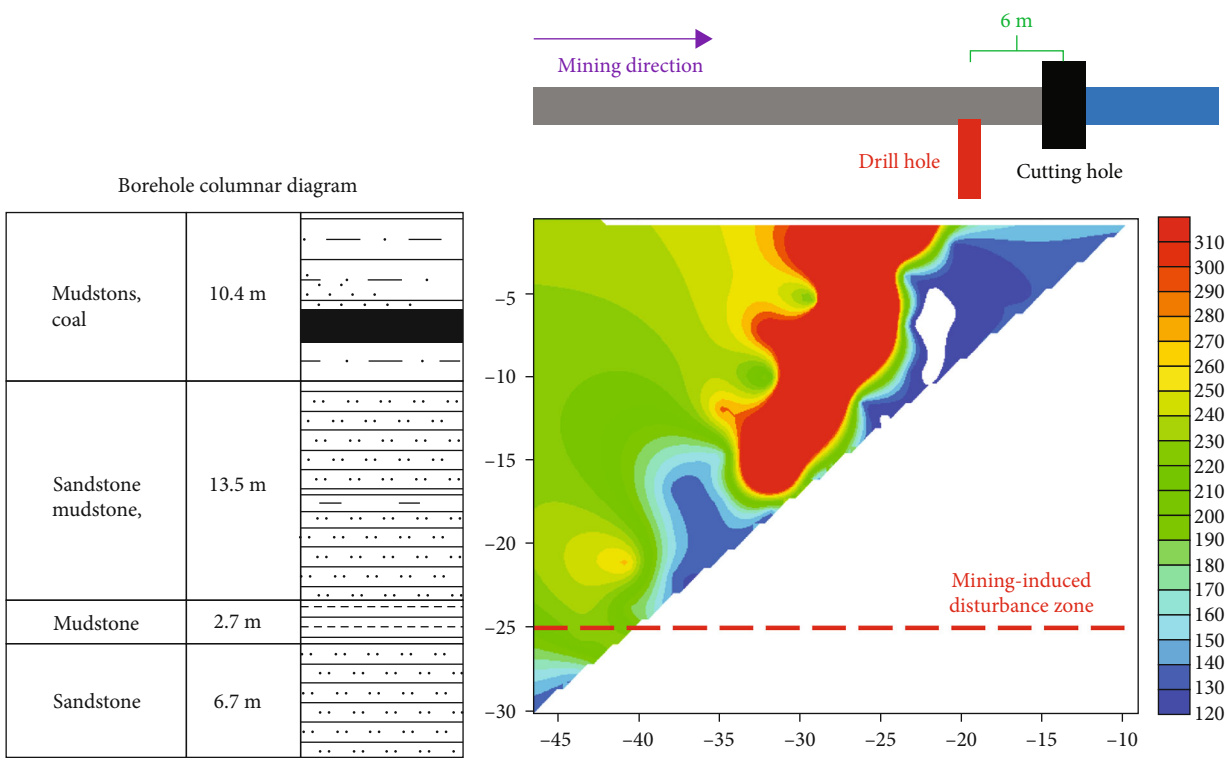

(b) On July 24

Figure 2: Continued.

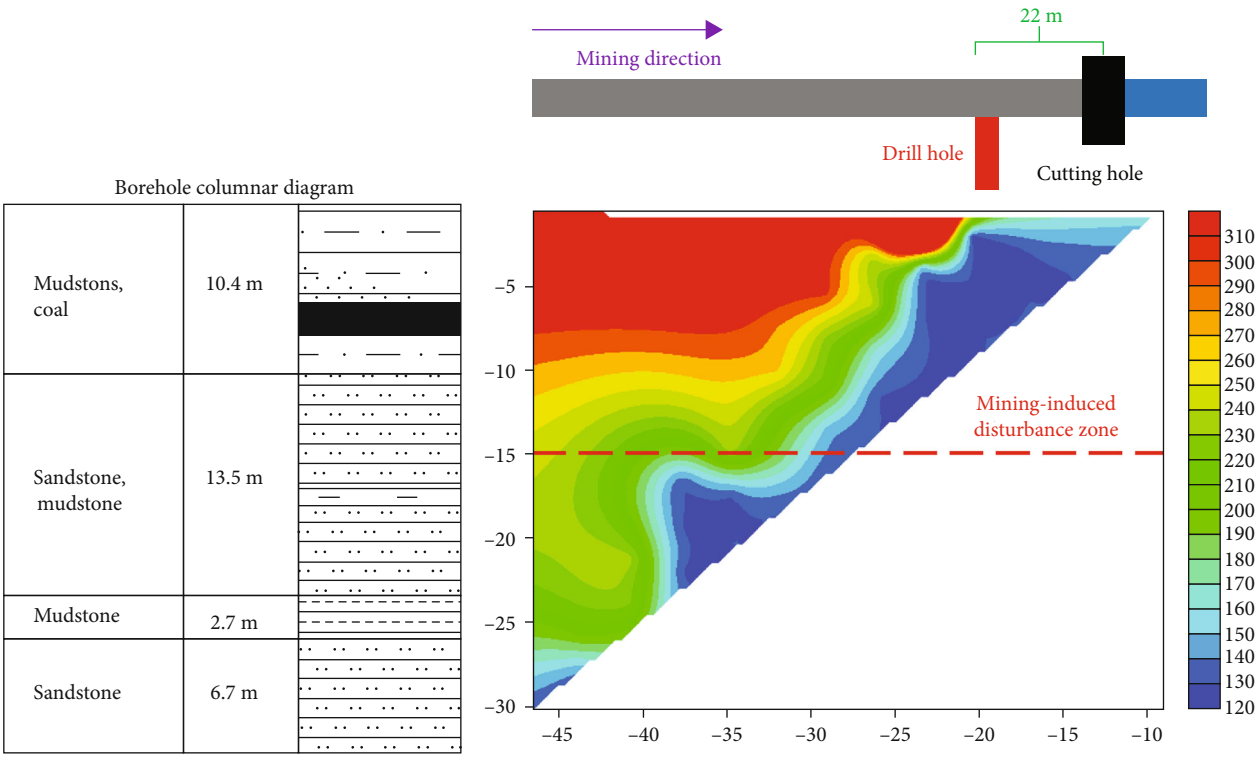

(c) On August 2

Figure 2: Apparent resistivity of borehole.

arbitrarily. AM method is to place the common power supply electrode B in an infinite distance; using a single-point power supply field power supply mode, the power supply electrode is circulated from the initial measuring point electrode to the end of the measuring point electrode; and other measuring electrodes collect the potential difference with the common reference electrode (N) in parallel. The electrodes on the measuring line of ABM method assume the power supply of A and B, and other measuring electrodes collect the potential difference with the common reference electrode (N) in parallel.

2.3. Numerical Simulation of Floor Failure of Working Face

2.3.1. Modeling. In order to further study and determine the floor failure characteristics of the working face and verify the field measurement results, the 61601 working face with different mining heights is simulated numerically through the simulation software FLAC (Fast Lagrangian Analysis for Continuum).

This numerical simulation corresponds as closely as possible to the field conditions. According to the previous data, it was known that the height of the water flowing fractured zone on the roof is about 165 m. In order to ensure the accuracy of the simulation and take into account the lithologic characteristics of the roof strata, the upper boundary of the model was set to 203 m, and the overlying strata are simplified as uniformly distributed loads acting to the top boundary of the model. The bottom boundary of the model was calculated to be 26.59 m as the floor failure depth of the 61601 working face according to the empirical formula in the specification for coal pillar retention and coal mining for buildings, water bodies, railways, and main roadways. According to the stratigraphic data, the floor failure depth did not affect the Ordovician limestone. However, in order to study the influence of floor failure depth on Ordovician limestone water, the bottom boundary of the model was selected to be 50 m below the top boundary of the Ordovician limestone. As a result, the lower boundary of the model was 95 m. A two-dimensional model was established according to the actual situation of the working face.

The entire model was 1000 m long and 322 m high and was divided into 32 strata and 23840 grids. The horizontal movement was restricted on both sides of this model, and the horizontal and vertical movement was restricted at the bottom of this model. The lithology of each stratum was set strictly according to the comprehensive column diagram of the working face, and the upper strata above the model were replaced by pressure. The mining started at 200 m from the mining direction of the working face in the No. 6 coal seam located at $J = 95\sim119$ m. The thickness and physical and mechanical parameters of each stratum were determined according to the measured data in Table 1. In order to correspond to the field observation, the vertical survey line was arranged at the corresponding position of the borehole in the underground electrical construction to monitor the stress changes at different depths in this position.

The ideal elastoplastic constitutive model, i.e., Mohr-Coulomb model, was used for calculation.

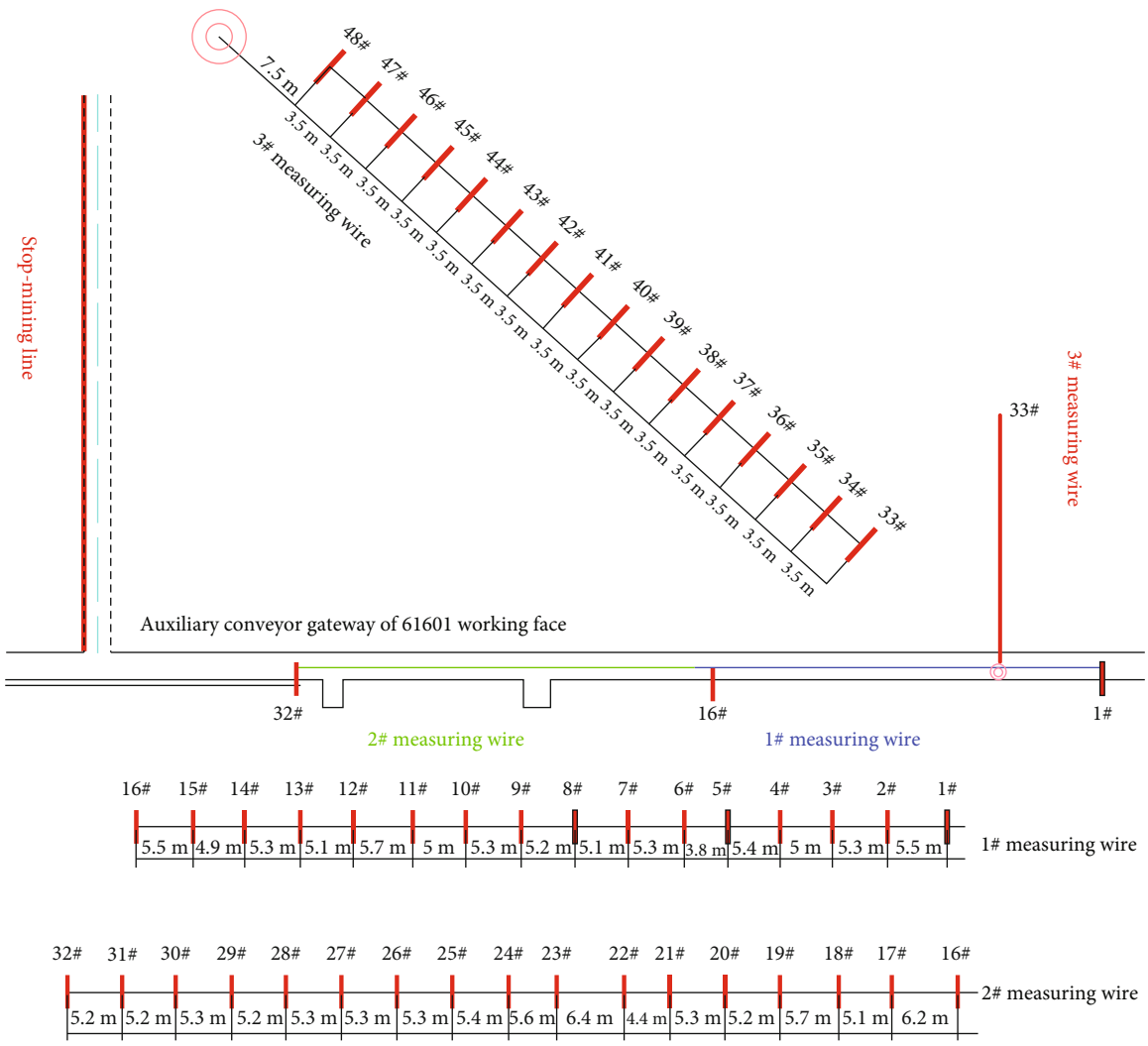

Figure 3: Layout of measuring wires and electrode positions.

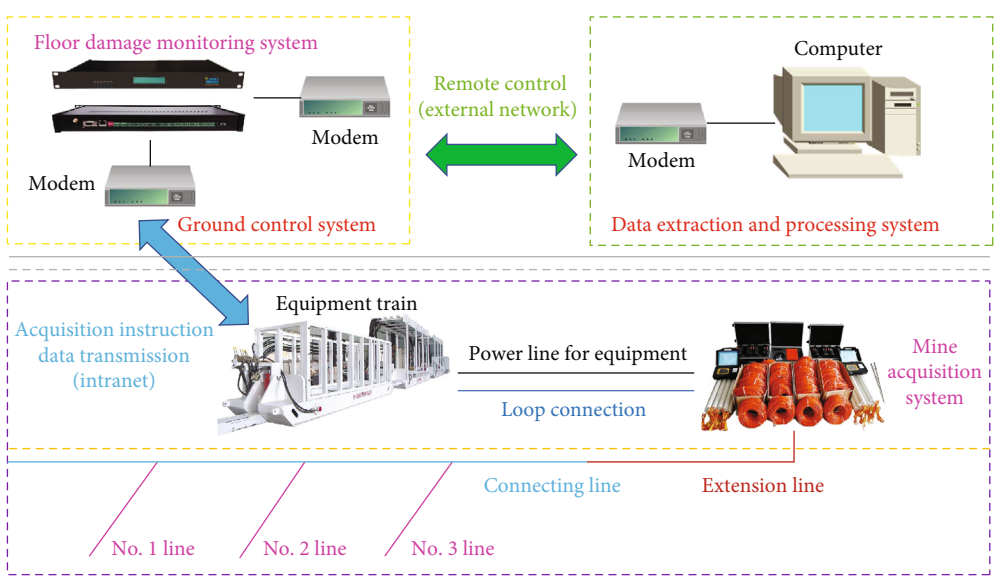

Figure 4: Schematic diagram of data acquisition system.

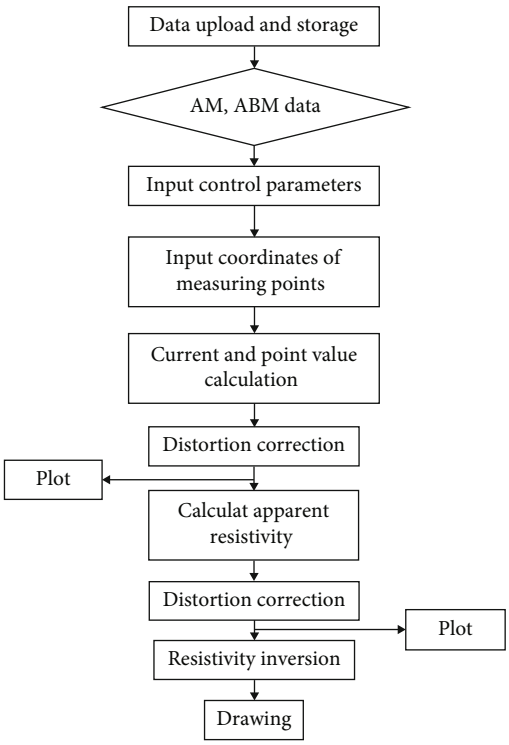

Figure 5: Data processing flowchart.

2.3.2. Numerical Simulation. The numerical simulation was conducted according to different mining heights: (1) 2 m, (2) 4 m, (3) 8 m, (4) 12 m, (5) 16 m, (6) 20 m, and (7) 24 m. After the model was established, the one-time full excavation method was adopted, i.e., one excavation from 200 m to 800 m in the mining direction of the working face, and the floor failure characteristics of the working face for the seven different mining heights were studied. During the simulation, the shear stress and shear strain were monitored in the area with a width of 12 m and a height of 10 m at both ends of the goaf floor, and a total of 28 points were monitored. Here, only the monitoring points on the left were listed, as shown in Figure 6. With the mining height of 24 m taken as an example, the area in the black box was the monitoring area, corresponding to the cells numbered 1~14.

3. Results

3.1. Field Measurement Results. According to relevant literature, the resistivity value of the floor of the working face changed as the mining process continued. A low-resistivity region appeared before the cutting hole (Figure 2(a)), indicating that this region was under compressive stress and advanced stress concentration occurred in this region. The goaf had high resistivity near the cutting hole and decreased resistivity away from the cutting hole (Figure 2(b)), which corresponded to the postmining pressure relief area and postmining stress recovery area, respectively. Regardless of whether it was in the advanced stress concentration region or the pressure relief region, if the change in resistivity did not exceed 20% with the depth of the floor of the working face greater than 25 m, it was considered that the change of less than 20% was a natural fluctuation in resistivity, and thus, the maximum depth of the floor disturbance zone could be considered to be 25 m. When the change in resistivity exceeded 40% with the depth of the floor of the working face less than 15 m and there was no recovery in the stress recovery zone (Figure 2(c)), it was considered that the floor within 15 m was damaged irreversibly by mining and it was the floor failure zone.

3.2. Numerical Simulation Results

3.2.1. Characteristics of Elastoplastic Zone. The variations of elastoplastic distribution under different mining height conditions were obtained through numerical simulation. Figure 7 shows the plasticity diagram for the floor failure of the working face with mining heights of 2 m, 12 m, and 24 m. For the mining height of 2 m, the plastic failure depth is 12~26 m, and it is about 18 m in most of the area. For the mining height of 12 m, the plastic failure depth is 12~21 m, and it is about 14 m in most of the area. For the mining height of 24 m, the plastic failure depth is 9~13 m, and it is about 11 m in most of the area. It is believed that the plastic change occurs in the floor failure of the working face. From the characteristics of the elastoplastic zone of the floor of the working face, it is obvious that the floor failure zone becomes smaller as the mining height increases.

3.2.2. Characteristics of Shear Stress. Through monitoring, it is found that the rules of stress and strain on the left and right sides are similar. Here, only the rules of stress and strain on the left are presented. Figure 8 shows the variation of shear stress with mining height in the monitoring area. It is indicated that the shear stress of the floor in the goaf shows a downward trend as the mining height increases.

3.2.3. Characteristics of Shear Strain. Figure 9 shows the variation of shear strain with mining height in the monitoring area. As the mining height increases from 2 m to 4 m, the shear strain increases. And then, as the mining height increases from 4 m to 12 m, the shear strain decreases significantly. Finally, as the mining height increases from 12 m to 24 m, the shear strain is basically unchanged with a slight increase. Generally, the shear strain of the floor in the goaf shows a downward trend.

3.3. Comparison and Analysis of Floor Failure Depth of Working Face

3.3.1. Reliability Analysis of Measured Results. The monitoring electrode was buried in the borehole and sealed with cement to ensure that the electrode was highly coupled with the surrounding rock. The electrode in the borehole was less interfered by equipment such as iron equipment in the working face. Due to the long monitoring period of the working face, the electrodes arranged under the floor of the roadway were affected by many factors such as the roadway cavity, equipment power supply, and disconnection, as well as the quality of natural potential and power supply current data. However, through the joint inversion calculation

Table 1: Physical and mechanical parameters of each stratum.

No.	Type	Thickness (m)	Bulk modulus (GPa)	Shear modulus (GPa)	Density (kg/m^3)	Tensile strength (MPa)	Cohesion (MPa)	Internal friction angle (°)
1	Limestone	50	24.56	21.59	2800	5.14	9.61	38
2	Bauxite mud	12	6.67	4	2700	0.85	4.61	29
3	Gritstone	7	8.22	5.91	2370	1.43	3.76	37
4	Mudstone	3	5	3.44	2330	0.56	2.65	26
5	Medium sandstone	4	7.04	5.5	2430	1.31	3.96	36
6	Mudstone	1	5	3.44	2370	0.56	2.65	26
7	Medium sandstone	6	7.04	5.5	2430	1.31	3.96	36
8	Mudstone	12	5	3.44	2370	0.56	2.65	26
9 ~ 15	No. 6 coal seam	24	0.43	0.19	1800	0.1	0.8	24
16	Sand slime stone interbedded	37	8.27	4.96	2570	1.25	4.34	36
17	Gritstone	14	9.48	6.82	2500	2.14	5.09	37
18	Mudstone	7	8.27	4.96	2570	1.25	4.34	36
19	Gritstone	9	9.48	6.82	2500	2.14	5.09	37
20	Mudstone	2	8.33	5	2570	1.31	4.64	32
21	Medium sandstone	4	9.69	6.38	2430	1.38	3.36	34
22	Mudstone	20	8.33	5	2570	1.31	4.64	32
23	Carbonaceous mudstone	11	8.46	5.57	1730	1.36	4.78	35
24	Mudstone	17	8.33	5	2570	1.31	4.64	32
25	Packsand	5	10.11	7.58	2460	1.66	4.05	38
26	Mudstone	9	8.33	5	2570	1.31	4.64	32
27	Gritstone	5	9.48	6.82	2370	1.49	3.62	36
28	Mudstone	5	8.33	5	2570	1.31	4.64	32
29	Gritstone	5	9.48	6.82	2370	1.49	3.62	36
30	Mudstone	9	8.33	5	2570	1.31	4.64	32
31	Gritstone	20	9.48	6.82	2370	1.49	3.62	36
32	Mudstone	24	8.33	5	2570	1.31	4.64	32

of drilling and roadway survey lines, combined with the natural potential and power supply current data of the roadway, the relatively real floor resistivity profile can be obtained, and the data were collected four times a day, mainly to verify the reliability of the data.

According to the field measurement above, the maximum depth of the floor failure zone was 15 m. The numerical simulation with the same mining height indicated that the plastic zone of the floor was 9~13 m. The instruments and methods for the electrical observation of the floor failure zone have good reliability because they have been practiced a lot in accordance with relevant specifications. In addition, since the numerical simulation was carried out with mature software, the simulation results are reliable. The results from the two methods can be mutually verified, indicating they have high reliability.

For Tangjiahui Coal Mine adjacent to the mine studied, the optical fiber sensing method was adopted for testing. It was found that the depths of the floor failure zone for the two working faces were 14.5 m and 16 m, respectively, which were similar to the results of this mine.

3.3.2. Comparison of Floor Failure Depth of Super-Large Mining Height Working Face with Previous Statistical Results. Previous researchers have conducted extensive investigations on the floor failure of the working face and proposed some statistical formulas. According to those statistical formulas, the depth of the floor failure zone of the working face was calculated based on the parameters of the working face (dip length L1 = 250 m, buried depth $H = 400$ m, dip angle $a = 2°$) for this mine, as shown in Table 2.

The four statistical formulas in Table 2 were all derived under the conditions of general mining height, reflecting the law of the floor failure zone of the working face with a general mining height (the mining height is generally not greater than 10 m). As shown in Table 2, the calculated results of the depth of the floor failure zone are all greater than the measured data (15 m) and numerically simulated data (11 m) of the 61601 working face in Longwanggou Coal Mine. This indicates that the depth of the floor failure zone of the working face with a super large mining height is smaller than that with a general mining height.

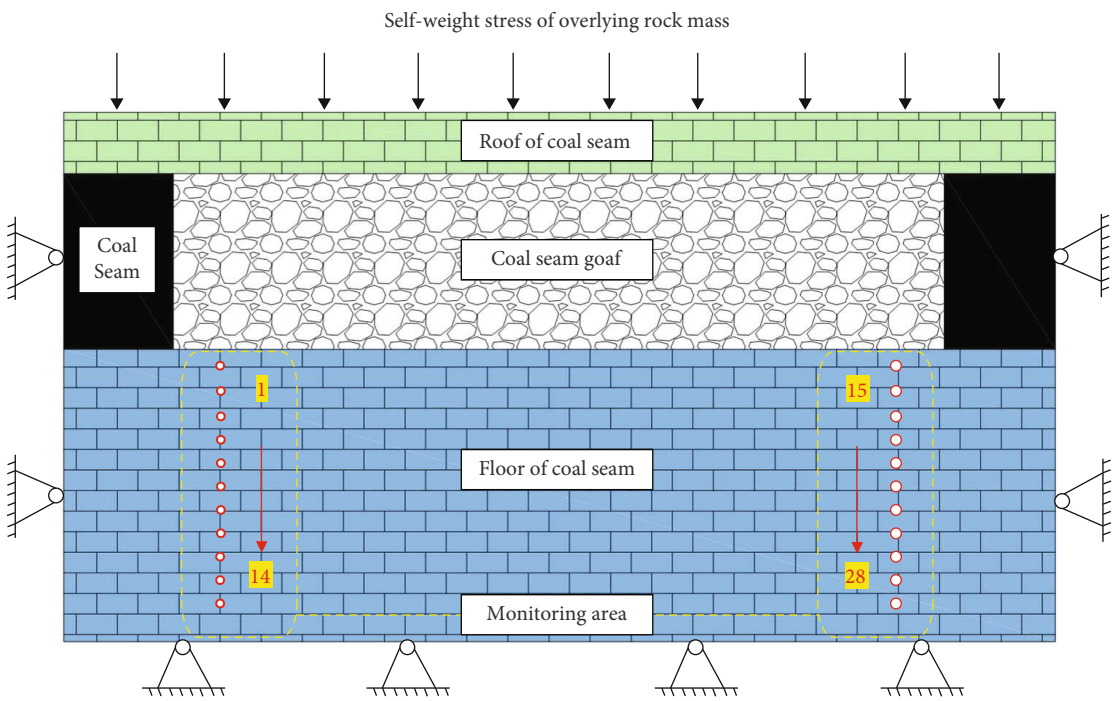

Figure 6: Shear stress and shear strain monitoring area.

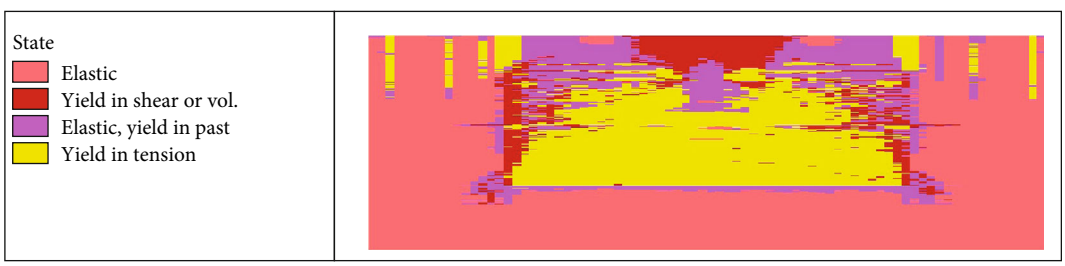

(a) Mining height = 2 m

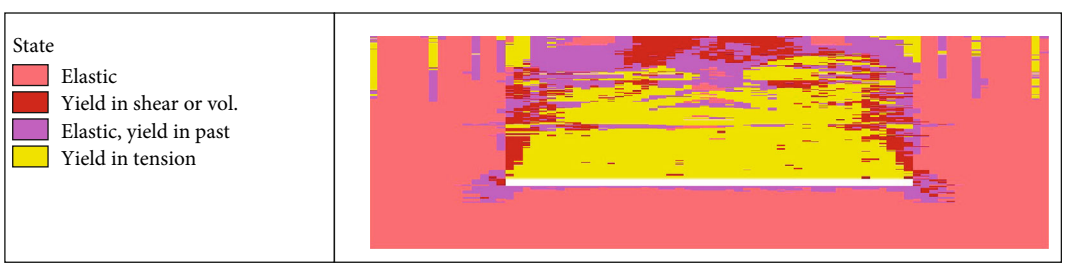

(b) Mining height = 12 m

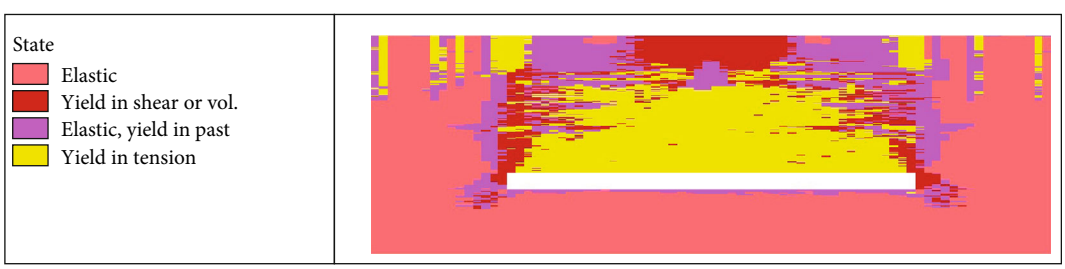

(c) Mining height = 24 m

Figure 7: Plasticity diagram for floor failure of working face.

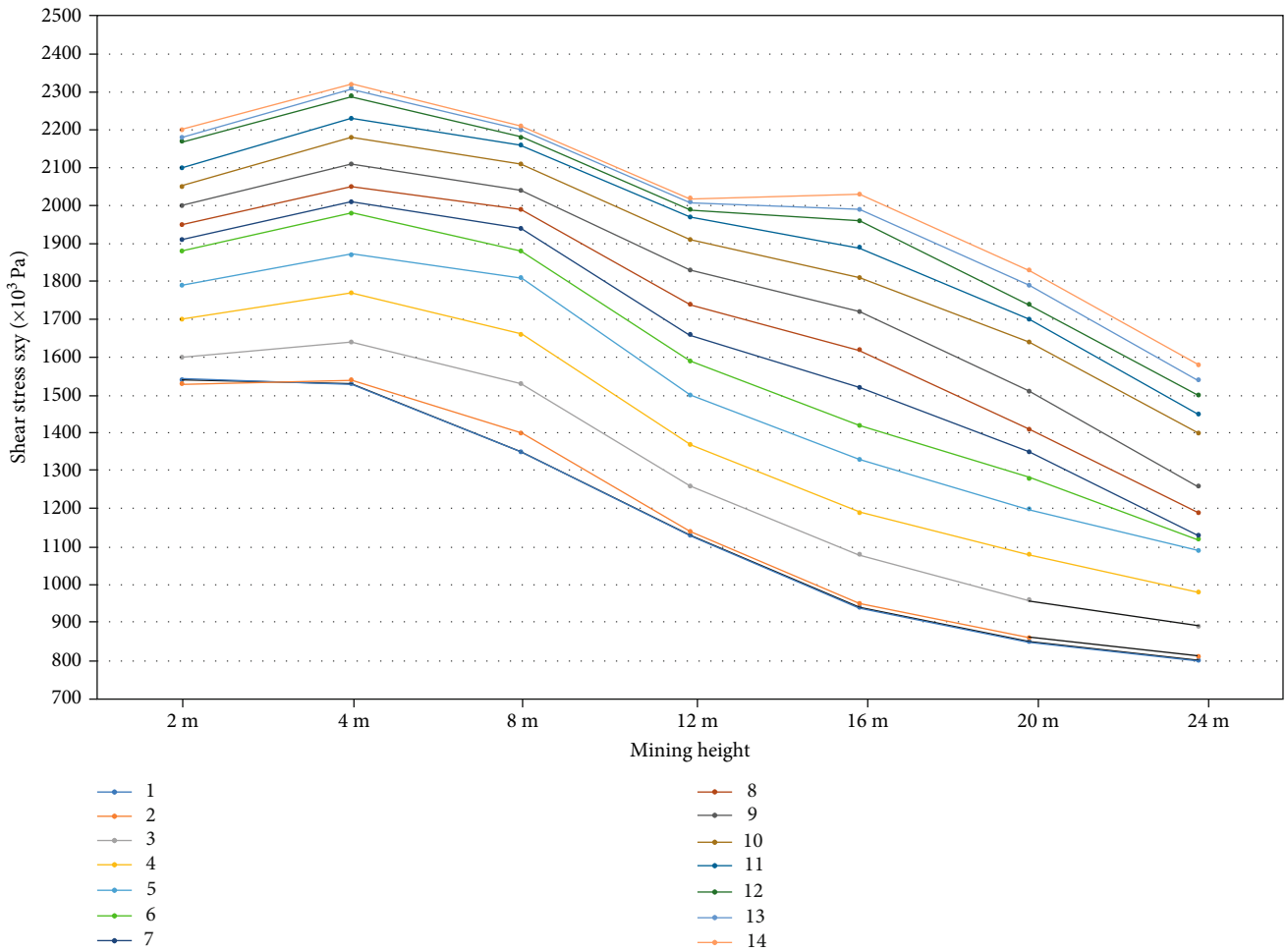

Figure 8: Variation of shear stress with mining heights in the monitoring area (1~14).

3.4. Theoretical Analysis of Floor Failure Depth of Super-Large Mining Height Working Face. The failure of the floor of the working face was due to the stress imbalance caused by mining activities.

According to the deformation characteristics of the floor under the force during mining, the floor can be divided into a compression zone and an expansion zone, as shown in Figure 2(c). The compression zone is located on both sides of the goaf, and the coal wall of the compression zone is subjected to additional downward vertical pressure (P). The expansion zone is located below the floor of the goaf, and it is subjected to an additional upward force (F) due to pressure relief.

For the working face with a general mining height, the mining height was not considered in the analysis and calculation of mining stress because the mining height has little effect on the floor failure zone of the working face. However, the mining height in Longwanggou Coal Mine is as high as 24 m, and thus, the influence of mining height cannot be ignored. Therefore, the influence of the mining height on the floor failure of the working face was analyzed theoretically as follows.

3.4.1. Influence of Falling Roof on Pressure Relief in the Goaf. As shown in Figure 2(c), when the working face is mined, the falling roof in the pressure relief zone has a downward gravity effect. The gravity is

$$G = \gamma h, \tag{1}$$

where h is the height of the caving zone (m). It can also be expressed as

$$G = \gamma n m, \tag{2}$$

where n is the ratio of falling to mining and m is the mining height (m). The direction of gravity of the falling roof is opposite to that of the additional stress generated by the pressure relief. With the gravity of the falling roof, the resultant upward force is decreased:

$$F_H = F - G = F - \gamma n m. \tag{3}$$

It is indicated that the greater the mining height, the greater the gravity of the falling roof, and the smaller the resultant upward force. Therefore, the gravity of the falling roof has an inhibitory effect on pressure relief. The greater the mining height is, the stronger the inhibition is, as shown in Figure 10.

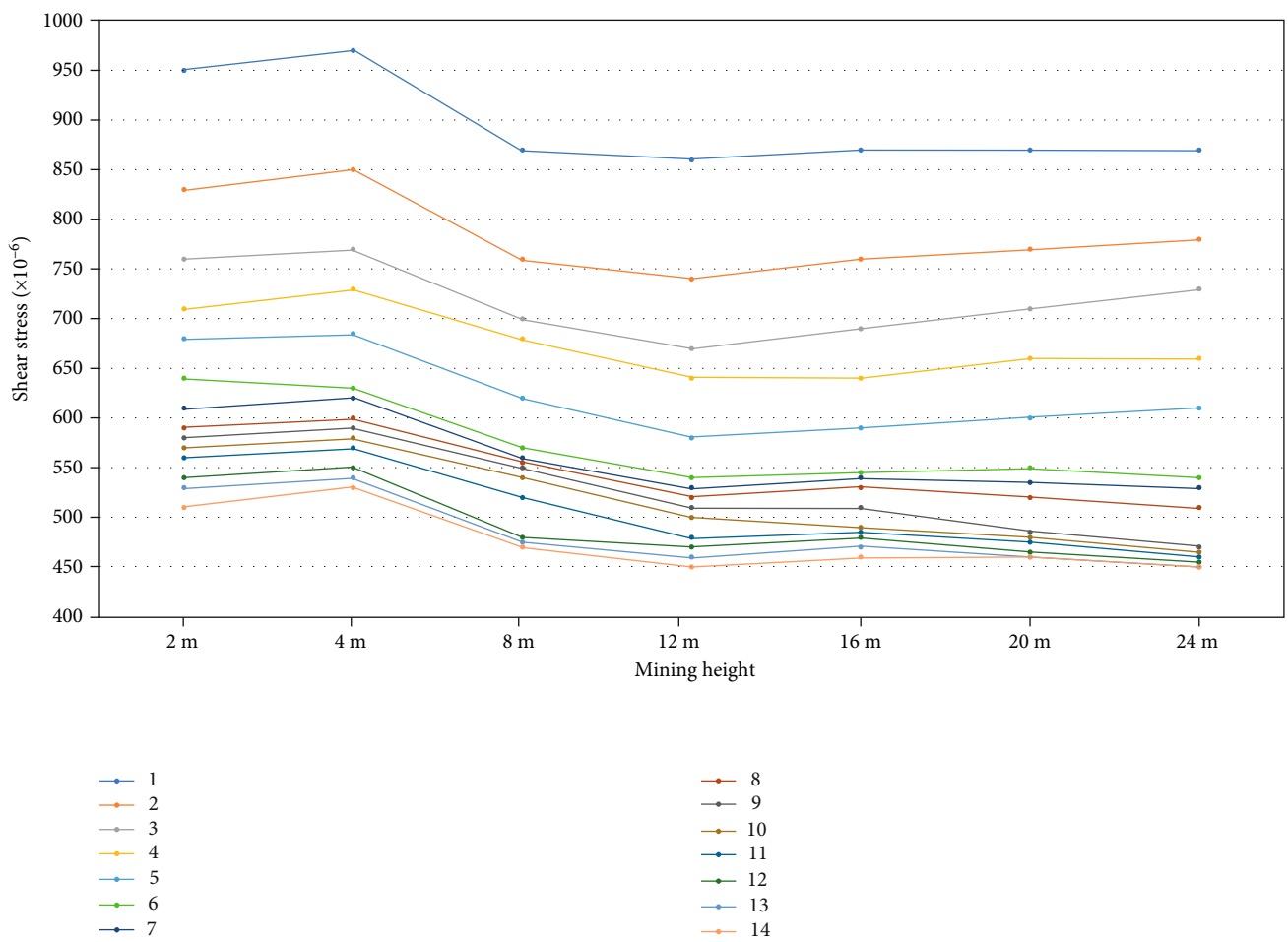

Figure 9: Variation of shear strain with mining height in the monitoring area (1~14).

Table 2: Depth of the floor failure zone of the working face calculated according to statistical formulas.

Source of formula	Formula	Depth of floor failure zone (m)
Li and Mi (1988) [1]	$h_d = 1.86 + 0.11\,L_1$	29.36
Wang et al. (2000) [29]	$h_d = 0.303\,L_1{}^{0.8}$	25.1
Zhang et al. (1997) [30]	$h_d = 3.2 + 0.085\,L_1$	24.45
"Lower three" procedure	$h = 0.0085H + 0.1665a + 0.1079\,L_1 - 4.3579$	26.35

3.4.2. Influence of Mining Height on Advanced Pressure. As shown in Figure 11, b is the working face width, m is the mining height, L is the length of the coal yield zone after the working face is mined, and h is the height of the caving zone. It is assumed that after the working face is mined, both the overlying rock mass that has not fallen on the working face and the rock mass in the yield zone are supported by the yield zone; i.e., there is advanced pressure in the yield zone.

Then, it can be obtained from the condition of static balance:

$$2L\gamma H + b\gamma(H - h) = 2LP. \tag{4}$$

Hence,

$$P = \gamma H + \frac{b\gamma(H - h)}{2L}, \tag{5}$$

where γ is the specific gravity of the overlying rock and P is the advanced pressure (MPa). In this formula, the height of the caving zone is $h = nm$, where n is the ratio of falling to mining. Therefore, Equation (5) can be rewritten as follows:

$$P = \gamma H + \frac{b\gamma(H - nm)}{2L}. \tag{6}$$

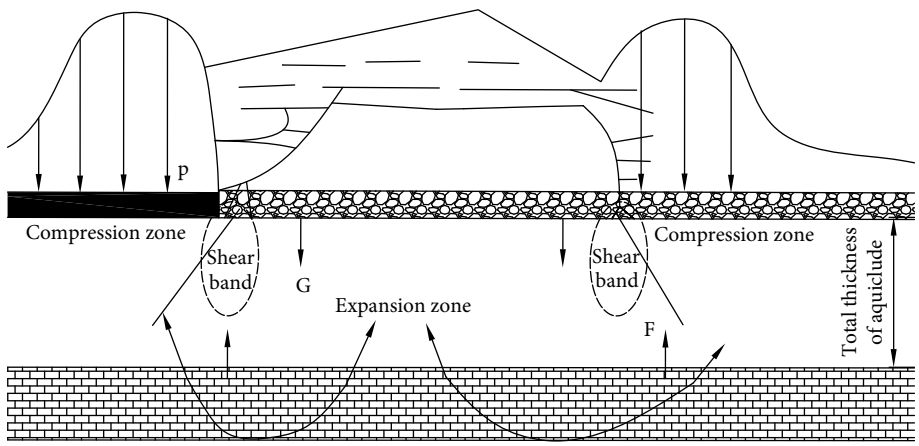

Figure 10: Distribution diagram of floor failure stress with influence of the falling roof considered.

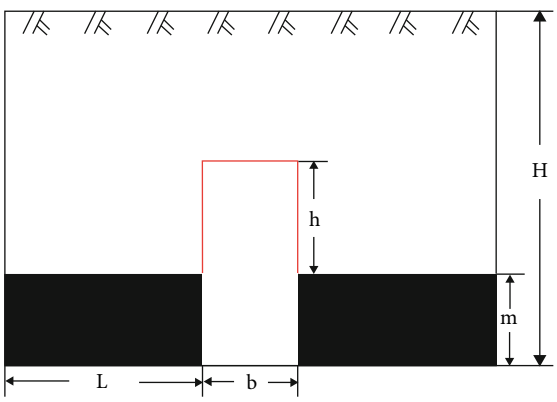

Figure 11: Schematic diagram of working face width, yield zone, and falling height.

According to the above equation, the advanced pressure of the working face is related to the mining height. The larger the mining height is, the smaller the advanced pressure is.

3.5. Comprehensive Analysis. From the analysis of the above two aspects, it is found that the mining height not only affects the advanced pressure but also affects the resultant upward force in the expansion zone. The larger the mining height is, the smaller the advanced pressure is, and the smaller the resultant upward force is in the expansion zone. The combined effect is to reduce the shear stress in the floor of the working face, which leads to a reduction in the size of the floor failure zone of the working face.

Since the mining height is smaller than the buried depth, the smaller mining height has less influence on the advanced stress, and the gravity of the falling roof is also limited. However, if the mining height is particularly large, its influence will exist to a certain extent. Because the mining height of this mine is 24 m, the influence of the mining height should exist.

4. Conclusions

Through the field measurement and numerical simulation of the 61601 working face with a mining height of 24 m in Longwanggou Coal Mine and the comparison and theoretical analysis of the obtained results, the following conclusions are drawn:

(1) The resistivity changes over 40% within the range of 15 m of the working face floor and does not recover; that is, the failure zone depth of the working face floor is 15 m

(2) The numerical simulation results show that the 9–13 m floor of the working face is a plastic failure zone, which is similar to the measured results and can be mutually verified with the measured results of adjacent mines

(3) The shear stress, shear strain, and size of the plastic failure zone of working face floor decrease with the increase of the mining height. The actual depth of floor failure of the super-large mining height working face is less than the calculation result of the statistical formula, and the calculation formula of the floor failure depth of the general mining height working face is no longer applicable

(4) The reason for the small failure zone of the floor in the super-large mining height working face is that the falling roof inhibits the pressure relief of the floor and the large mining height reduces the advanced pressure, thereby reducing the shear stress of the floor

(5) The danger of water inrush from the floor of the working face with a super-large mining height is not more serious than that with a general mining height

Data Availability

The data used to support the findings of this study are included within the article.

Conflicts of Interest

We declare that we have no conflict of interest.

Acknowledgments

The research was supported by the National Key Research and Development Program of China (No. 2019YFC1805400) and the National Natural Science Foundation of China (No. 42174165).

References

[1] B. Y. Li and S. Z. Mi, "Mining engineering hydrogeology," *Teaching Material of Shandong Mining Institute*, pp. 20–50, 1988.

[2] B. Y. Li, G. H. Shen, Z. G. Jing, and H. Gao, "Theory and practice of preventing water inrush from floor of mining face," *Coal Mine Safety*, vol. 5, pp. 47-48, 1988.

[3] X. G. Li and Y. F. Gao, "Influence of mining on floor infiltration coefficients," *Chinese Journal of Rock Mechanics and Engineering*, vol. 22, no. 7, pp. 1078–1082, 2003.

[4] G. Zheng, Y. M. Meng, and X. Q. Pang, "On time monitoring and measuring technology before water inrush disaster occurred from floor of No19103 coal mining face in Dongpang Mine," *Coal Science and Technology*, vol. 32, no. 3, pp. 4–7, 2003.

[5] J. P. Xu, W. H. Sui, H. Gui, and Y. D. Zhang, "Utilizing angular displacement to monitor failure of coal seam floor," *Procedia Earth and Planetary Science*, vol. 1, no. 1, pp. 943–948, 2009.

[6] S. D. Liu, B. Wang, G. Q. Zhou, S. L. Yang, and M. J. Chen, "Experimental research on mine floor water hazard early warning based on response of geoelectric field in groundwater seepage," *Chinese Journal of Rock Mechanics and Engineering*, vol. 28, no. 2, pp. 267–272, 2009.

[7] X. M. Zhang, K. J. Yu, J. D. Xi et al., "Research and application of microseismic technique in monitoring "two zones" in coal mine," *Journal of China Coal Society*, vol. 25, no. 6, pp. 334–338, 2000.

[8] M. Shahriari, D. Pardo, A. Picon, A. Galdran, J. del Ser, and C. Torres-Verdín, "A deep learning approach to the inversion of borehole resistivity measurements," *Computational Geosciences*, vol. 24, no. 3, pp. 971–994, 2020.

[9] W. L. Zhou, P. S. Zhang, R. X. Wu, and X. Hu, "Dynamic monitoring the deformation and failure of extra-thick coal seam floor in deep mining," *Journal of Applied Geophysics*, vol. 163, pp. 132–138, 2019.

[10] K. Ma, X. Y. Sun, C. A. Tang, F. Z. Yuan, S. J. Wang, and T. Chen, "Floor water inrush analysis based on mechanical failure characters and microseismic monitoring," *Tunnelling and Underground Space Technology*, vol. 108, article 103698, 2021.

[11] X. L. Wang, *Frack evolution and destruction characteristics of mining bottom plate on pressurized water based on similar simulation*, Geotechnical and Geological Engineering, 2021.

[12] B. Y. Sun, P. S. Zhang, and M. R. Fu, "Comparative study on the "optic-electric" monitoring method for the deformation and failure of surrounding rock in stopes," *Natural Hazards*, vol. 110, no. 1, pp. 407–427, 2022.

[13] K. P. Zhu, X. M. Huang, and Y. Liu, "Numerical simulation analysis of relation between mining width of working face and depth of mining failure zone of coal floor," *Coal Mining Technology*, vol. 14, no. 4, pp. 74–77, 2009.

[14] X. Li, S. Chen, Q. Zhang, X. Gao, and F. Feng, "Research on theory, simulation and measurement of stress behavior under regenerated roof condition," *Geomechanics and Engineering*, vol. 26, no. 1, pp. 49–61, 2021.

[15] Z. N. Gao and X. R. Meng, "Study on deformation and failure characteristics of coal seam floor under mining conditions," *Mining Safety & Environmental Protection*, vol. 37, no. 3, pp. 17–24, 2010.

[16] B. L. Zhang and Z. B. Meng, "Experimental study on floor failure of coal mining above confined water," *Arabian Journal of Geosciences*, vol. 12, no. 4, 2019.

[17] Y. B. Guan, H. M. Li, and J. C. Lu, "Research of No•9coal seam floor's fracture regularity in Xiandewang Coal Mine," *Journal of China Coal Society*, vol. 28, no. 2, pp. 121–125, 2003.

[18] H. F. Duan, Z. Q. Jiang, S. Y. Zhu et al., "Measurement of mining-induced floor failure regularity for thin coal seams using fully mechanized coal caving," *Journal of Mining & Safety Engineering*, vol. 28, no. 3, pp. 407–414, 2011.

[19] R. Q. Zuo, X. N. Gong, and H. R. Gui, "Study on the deformation and failure rules of coal seam floor under the influence of multiple factors," *Coal Technology of Northeast China*, vol. 5, pp. 3–7, 1999.

[20] W. T. Liu, D. R. Mu, L. Yang, L. Y. Li, and C. H. Shi, "Calculation method and main factor sensitivity analysis of inclined coal floor damage depth," *Journal of China Coal Society*, vol. 42, no. 4, pp. 849–859, 2017.

[21] S. H. Sun, L. Su, and Z. Y. Su, "Influence of dip angle of coal seam on failure zone depth of floor," *Coal*, vol. 26, no. 8, pp. 29–32, 2017.

[22] J. Li, Y. Xu, X. Xie, Y. Yao, and Y. Gao, "Influence of mining height on coal seam floor failure depth," *Journal of China Coal Society*, vol. 40, no. S2, pp. 303–310, 2015.

[23] X. L. Li, S. J. Chen, S. M. Liu, and Z. H. Li, "AE waveform characteristics of rock mass under uniaxial loading based on Hilbert-Huang transform," *Journal of Central South University*, vol. 28, no. 6, pp. 1843–1856, 2021.

[24] S. Y. Zhu, D. T. Cao, Z. C. Yue et al., "Comprehensive measurement of characteristics of deformation and failure of extra-thick coal seam floor induced by fully mechanized top-coal mining," *Chinese Journal of Geotechnical Engineering*, vol. 34, no. 10, pp. 1931–1938, 2012.

[25] Z. C. Ren and N. Wang, "The overburden strata caving characteristics and height determination of water conducting fracture zone in fully mechanized caving mining of extra thick coal seam," *Geotechnical and Geological Engineering*, vol. 38, no. 1, pp. 329–341, 2020.

[26] D. Z. Kong, Y. H. Lou, S. S. Zheng, and S. Pu, "The characteristics of roof breaking and the law of ground pressure behavior in fully mechanized top-coal caving face with large mining height," *Geotechnical and Geological Engineering*, vol. 39, no. 1, pp. 285–297, 2021.

[27] S. D. Liu, "Technical system and new progress of mine parallel electrical method," *Journal of Coal*, vol. 44, no. 8, pp. 2336–2345, 2019.

[28] B. Wang, S. D. Liu, and P. Zhang, "Dynamic monitoring of coal mine floor using network parallel electrical instrument," *China Coal Geology*, vol. 21, no. 3, pp. 59–63, 2009.

[29] X. L. Wang, J. M. Liang, and J. X. Wang, "Test study on coal seams floor destroyed deepth under different mining condition," *Coal*, vol. 9, no. 3, pp. 22–24, 2000.

[30] J. C. Zhang, Y. Z. Zhang, and T. Q. Liu, *Rock Seepage and Water Inrush from Floor of Coal Seam*, Geological Publishing House, Beijing, China, 1997.